Carbonaceous Mudstone Hosting the Eskay Creek Deposit, Northwestern British Columbia (NTS 104B/09, /10): Multivariate Statistical Analysis of Compositional Trends

T. Meuzelaar, Department of Geology and Geological Engineering, Colorado School of Mines, Golden, CO, tmeuzela@mymail.mines.edu

T. Monecke, Department of Geology and Geological Engineering, Colorado School of Mines, Golden, CO

Meuzelaar, T. and Monecke, T. (2011): Carbonaceous mudstone hosting the Eskay Creek deposit, northwestern British Columbia (NTS 104B/09, /10): multivariate statistical analysis of compositional trends; *in* Geoscience BC Summary of Activities 2010, Geoscience BC, Report 2011-1, p. 45–56.

Abstract

Eskay Creek represents an unusual, precious metal-rich, polymetallic, volcanic-hosted sulphide and sulphosalt deposit located in the Iskut River area of northwestern British Columbia. The bulk of the ore consists of stratiform clastic beds and laminations of graded sulphide and sulphosalt debris that are hosted by a thick interval of carbonaceous mudstone at the contact between felsic volcanic rocks and overlying basalt. In addition to the stratiform orebodies, economic concentrations of precious metals have been recognized in discordant zones of sulphide veins and disseminations in the footwall rhyolite.

Detailed compositional investigations of the carbonaceous mudstone hosting the stratiform ores at Eskay Creek reveal the existence of a distinctive alteration halo around the deposit. Interaction of the host mudstone with hydrothermal fluids resulted in the widespread formation of carbonate minerals. Qualitative and quantitative X-ray diffraction analysis showed that altered mudstone contains abundant ankerite, with ferroan magnesite, magnesian siderite and siderite being locally present. Calcite was found to occur in the outer part of the alteration halo and forms an important component of mudstone away from the deposit. Carbonate alteration of the mudstone was accompanied by the formation of kaolinite. The spatial distribution of the different carbonate species suggests that carbonate alteration of the fine-grained carbonaceous hostrocks was largely restricted to areas overlying upflow zones of mineralizing hydrothermal fluids and associated discordant sulphide zones in the footwall rhyolite. Fluid-rock interaction and associated carbonate alteration in the halo around the deposit are interpreted to have taken place in seawater-saturated mudstone at low to moderate temperatures from cooling, low-pH, high-CO_2 fluids.

Principal-component analysis of the geochemical dataset provides support for carbonate-alteration trends observed by whole-rock XRD analysis and reveals additional mineralogical and component vectors to ore, including increasing Mg/F ratios in chlorite, increasing V/C_{org} ratios in the mudstone and variable Cs substitution ratios in white mica, all proximal to hydrothermal activity. Arsenic concentrations in pyrite also increase towards mineralized zones and can be used to discern hydrothermal from diagenetic pyrite.

Keywords: *Eskay Creek, geochemistry, carbonaceous mudstone, gold, massive sulphides, ore vector, carbonate alteration, multivariate statistical analysis, principal-component analysis*

This publication is also available, free of charge, as colour digital files in Adobe Acrobat® PDF format from the Geoscience BC website: http://www.geosciencebc.com/s/DataReleases.asp.

Purpose of Research

The Eskay Creek deposit (MINFILE 104B 008; BC Geological Survey, 2010) in northwestern BC has generated significant interest because it is among the most precious metal–rich volcanic-hosted massive-sulphide deposits in the world (48.4 g/t Au and 132.3 g/t Ag), and several of its geological characteristics differ from ordinary massive-sulphide deposits. Key features include the bedded and commonly graded nature of the clastic ore; the high concentrations of Au, Ag and other elements more typically associated with epithermal environments; the complex ore mineralogy; and the low temperatures (<200°C) of sulphide and sulphosalt deposition (Roth et al., 1999). The deposit has been considered a type example of a new group of volcanic-hosted gold deposits that formed in relatively shallow water submarine environments where phase separation of the hydrothermal fluids represented an important control on the precipitation of metals (Hannington et al., 1999).

Economic concentrations of precious and base metals at Eskay Creek are confined mainly to laterally discontinuous, stratiform clastic ore lenses hosted by a thick mudstone interval at the contact between felsic volcanic rocks and overlying basalt. Although the mineralizing hydrothermal system was active over an extensive area, it is currently not well established whether mineralogical gradients within ei-

ther the footwall alteration halo or the mudstone hosting the sulphides can be used for target vectoring. Due to the absence of readily recognizable alteration features in the carbonaceous mudstone, previous research focused largely on hydrothermal alteration patterns in the footwall rhyolite (Barrett and Sherlock, 1996).

This paper reports initial results of a comprehensive mineralogical and geochemical study of the ore-hosting mudstone, and demonstrates that hydrothermal alteration can be recognized up to tens to hundreds of metres from the orebodies. Identification of compositional gradients within the alteration halo permits the delineation of a set of vectors to ore that can be used in the exploration for this unusual deposit type in BC and elsewhere.

Geology

The Eskay Creek deposit is located in the Iskut River area at the western margin of the allochthonous Stikine terrane of the northern Canadian Cordillera (Figure 1). Middle Jurassic submarine and subaerial volcanic and sedimentary rocks in the Iskut River area have yielded U-Pb zircon ages between 181 and 172 Ma (Childe, 1996). The hostrocks of the deposit are folded into a shallowly north-plunging, north-northeast-trending, upright open anticline (Figure 1). Stratiform mineralization at Eskay Creek occurs on the western limb of the fold, near the fold closure, and dips gently 30–45 to the west (Figure 2). The metamorphic grade in the mine area is lower greenschist (Britton et al., 1990; Roth et al., 1999).

The stratigraphic footwall to the mineralization is composed of multiple intrusive/extrusive rhyolite units with a maximum apparent thickness of approximately 100 m in the mine area. Hydrothermal alteration is widespread throughout the footwall rhyolite. Secondary potassium-feldspar alteration and moderate silicification occur peripheral to the stratiform ore and in deeper parts of the footwall. Immediately underlying the stratiform ores, a more intense and texturally destructive alteration is seen in a tabular zone of pervasive chlorite and white-mica formation (Barrett and Sherlock, 1996; Monecke et al., work in progress).

The footwall rhyolite is overlain by carbonaceous mudstone, which hosts the clastic sulphide and sulphosalt orebodies. The unit ranges from <1 to >60 m in thickness. The mudstone is laminated, thinly bedded or massive, and contains abundant intercalated, tan-coloured beds of fine-

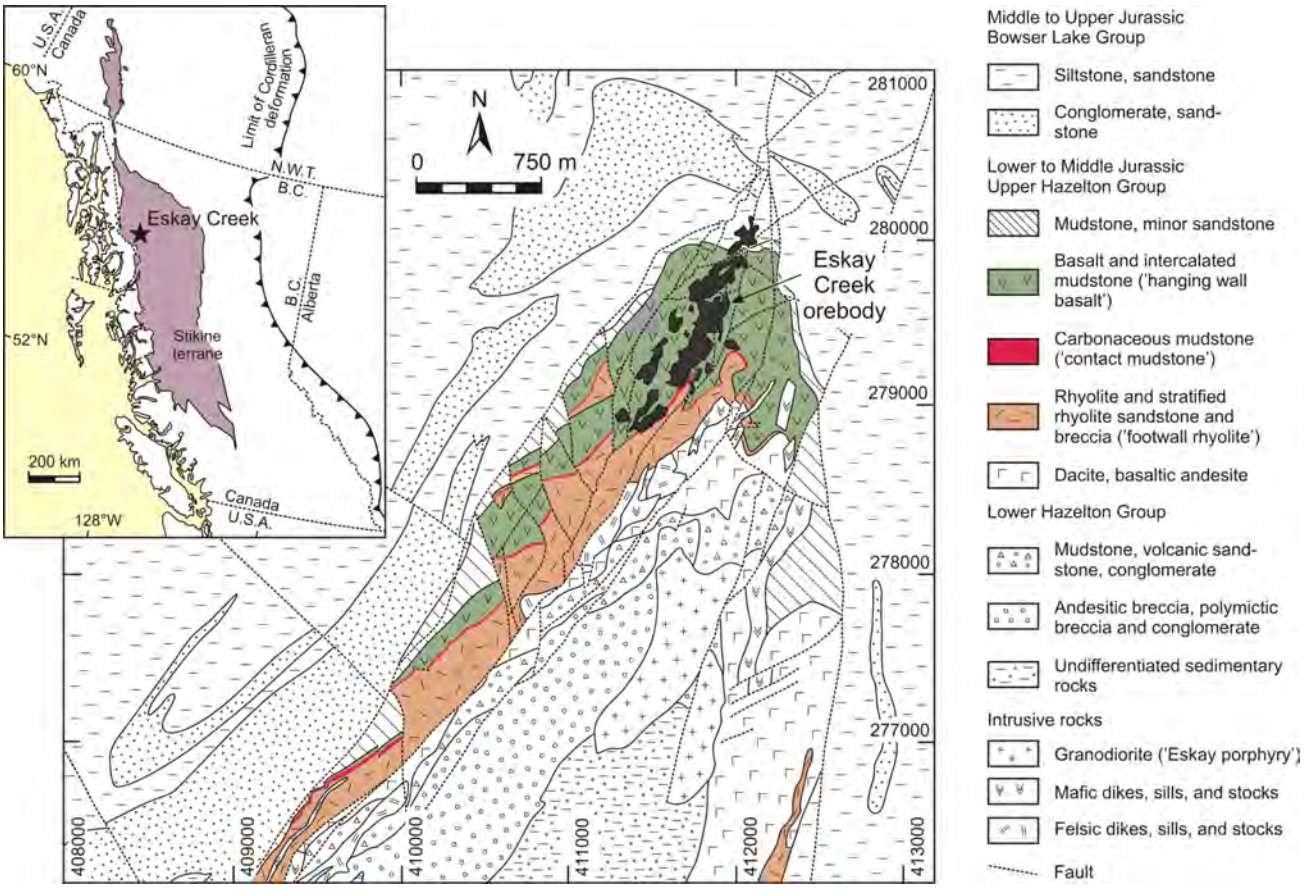

Figure 1. Geology of the Eskay Creek anticline, showing the locations of the surface projection of the ore zones (modified from Alldrick et al., 2005). Inset shows the location of the deposit in the Stikine terrane (modified from Gabrielse et al., 1991).

grained volcaniclastic material. Calcareous and siliceous intervals can be recognized in drillcore but are not common. The mudstone unit contains radiolarians, dinoflagellates, rare belemnites and corals, confirming a marine depositional environment. Thin pyrite laminations are common within the mudstone. The occurrence of flame structures at the base of the sulphide laminations indicates that this type of pyrite is clastic in origin. Additionally, thin veins and veinlets of pyrite crosscutting bedding are widespread throughout the mine area. Diagenetic pyrite nodules have been locally observed (Monecke et al., 2005).

Basalt sills and dikes occur throughout the carbonaceous mudstone unit. The occurrence of mudstone-matrix basalt breccia along the bottom and top margins of coherent basalt intervals indicates that the lava intruded mudstone that was still wet and unconsolidated (Monecke et al., 2005). The relative proportion of basalt increases in the upper part of the mine succession. The hangingwall basalt locally exceeds 150 m in thickness and generally thins southward away from the deposit. The mafic rocks are intercalated with variably thick intervals of the carbonaceous mudstone.

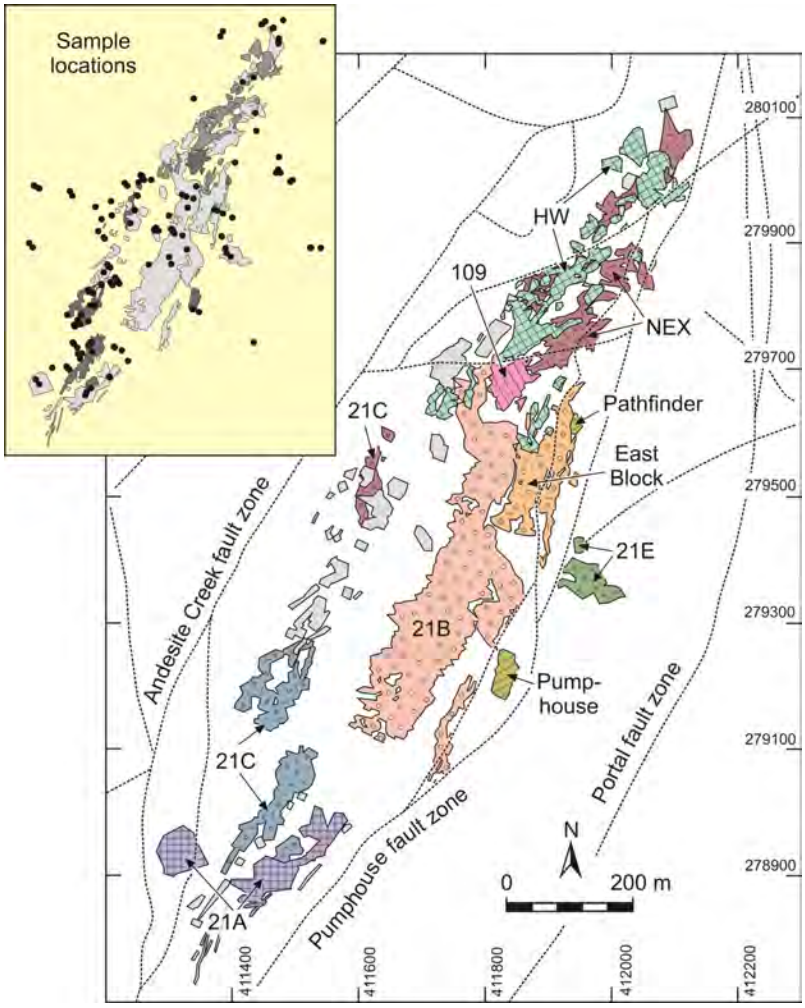

Figure 2. Plan view of the spatial distribution of mineralized zones at Eskay Creek (modified from Roth et al., 1999). Inset shows the projected locations of mudstone samples investigated in this study. Note that additional samples were collected outside the immediate deposit area.

Mudstone Mineralogy

One hundred and eighty mudstone samples were selected from exploration drillcore, as well as surface and underground exposures (Figure 2, inset). The samples were collected at various distances from ore, ranging from the immediate ore zones to a maximum distance of approximately 4.4 km from ore. Mudstone samples were further subdivided into contact and hangingwall mudstones. The contact mudstone unit is defined as the mudstone between the upper surface of the footwall rhyolite and the lowest basalt unit in the hangingwall. Mudstone occurring farther up stratigraphy in the mine succession is collectively referred to as the hangingwall mudstone.

Qualitative and quantitative X-ray powder diffraction (XRD) analysis, using the Rietveld method, identified 28 different minerals within the mudstone samples and revealed that the hostrocks of the stratiform mineralization have a highly variable mineralogical composition. Analytical results for the 180 samples collected from the contact and hangingwall mudstones are summarized in a series of histograms (Figure 3). The mineralogical compositions of representative samples are listed in Table 1.

Mudstones from Eskay Creek contain abundant quartz, plagioclase and microcline (Figure 3). Some contact mudstone contains anomalously high quartz contents (50–80 wt. %) when compared to mudstone from the hangingwall (rarely >50%). The observed variations in quartz content may reflect differences in protolith composition, or alternatively result from hydrothermal alteration of the contact mudstone. Another possible indication for mineralogical changes caused by fluid-rock interaction is the generally lower plagioclase content of the contact mudstone.

Carbonate minerals are a significant component of the mudstones hosting the Eskay Creek deposit, sometimes exceeding 30 wt. %. Stratiform ore at Eskay Creek is laterally discontinuous and carbonate abundances did not initially appear strongly correlated to mineralization. Scatter diagrams suggest only a weak correlation between increased

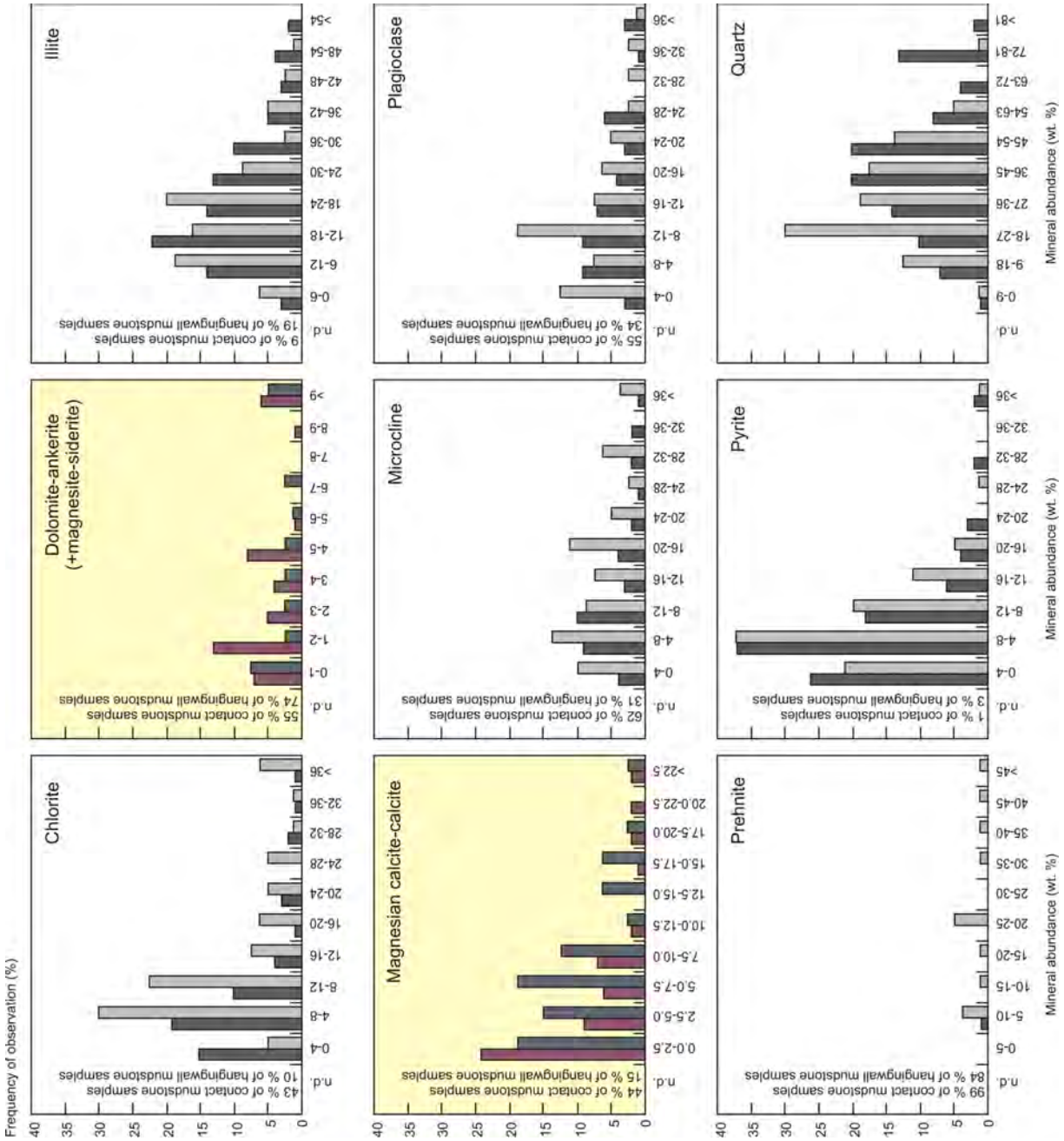

Figure 3. Histograms depicting the occurrence of rock-forming minerals in the contact and hangingwall mudstones of the Eskay Creek deposit. Contact mudstone is typified by a higher quartz concentration and commonly contains members of the dolomite-ankerite and magnesite-siderite solid solutions. Samples collected from the stratigraphically higher hangingwall mudstone are characterized by elevated chlorite and feldspar contents, and contain abundant prehnite in proximity to basaltic intrusions.

Table 1. Mineralogical composition (wt. %) of representative mudstone samples from the Eskay Creek deposit ('–' indicates not detected or not present)

Sample number	Distance (m)[1]	Anatase	Ankerite[2]	Calcite	Chlorite	Illite[3]	Microcline	Plagioclase	Prehnite	Pyrite	Quartz	Siderite[4]	Sphalerite
Contact mudstone													
U047-050	1	0.5 ±0.2	14.2 ±1.0	–	13.3 ±1.1	29.0 ±2.5	–	–	–	9.6 ±0.4	33.4 ±1.0	–	–
AD9763-388	4	–	–	0.5 ±0.3	–	10.7 ±1.7	–	1.4 ±0.5	–	22.4 ±0.4	65.0 ±0.8	–	–
C99973-160	7	–	–	–	–	44.5 ±4.3	–	–	–	5.1 ±0.3	50.4 ±1.3	–	–
AD9761-411	15	–	2.1 ±0.3	–	–	8.6 ±0.9	–	8.5 ±0.9	–	6.7 ±0.2	74.1 ±1.1	–	–
C99958-149	21	0.3 ±0.2	–	–	–	36.8 ±2.9	4.7 ±0.8	–	–	6.6 ±0.4	51.6 ±1.2	–	–
C96783-098	149	0.7 ±0.2	1.8 ±0.5	4.1 ±0.3	–	6.7 ±1.0	–	41.4 ±1.0	–	15.6 ±0.4	29.7 ±0.8	–	–
C96738-124	200	0.6 ±0.2	2.0 ±0.4	8.7 ±0.4	–	6.2 ±0.9	–	25.2 ±1.0	–	11.9 ±0.3	45.4 ±0.9	–	–
C96738-111	205	0.7 ±0.2	4.9 ±0.6	11.8 ±0.5	–	13.9 ±2.0	–	16.1 ±1.0	–	11.8 ±0.3	40.8 ±1.0	–	–
C98919-043	759	0.7 ±0.2	2.8 ±0.4	1.0 ±0.2	–	30.6 ±2.6	7.1 ±0.8	12.0 ±1.1	–	11.2 ±0.5	32.4 ±0.9	1.7 ±0.4	0.5 ±0.2
MP9808-273	4,425	–	–	0.4 ±0.2	–	32.5 ±2.1	36.1 ±1.2	–	–	0.4 ±0.1	29.2 ±0.8	1.4 ±0.2	–
Hangingwall mudstone													
C99961-132	11	0.5 ±0.3	–	2.4 ±0.3	12.4 ±1.3	16.9 ±2.3	19.3 ±1.0	8.5 ±0.9	–	12.8 ±0.4	27.2 ±1.0	–	–
C99973-115	23	0.3 ±0.2	0.5 ±0.4	5.9 ±0.5	9.9 ±1.0	7.6 ±1.3	26.2 ±1.1	18.9 ±1.1	–	4.0 ±0.3	26.7 ±0.9	–	–
CA90271-096	39	0.6 ±0.3	–	12.9 ±0.5	20.6 ±0.9	17.9 ±2.3	–	5.5 ±0.6	–	3.2 ±0.2	39.3 ±0.8	–	–
AD9769-402	50	–	–	1.1 ±0.5	32.2 ±1.6	–	10.2 ±1.5	2.5 ±1.0	22.0 ±1.3	16.7 ±0.7	15.3 ±1.1	–	–
C96786-060	62	–	–	2.0 ±0.3	17.1 ±0.9	–	22.3 ±1.0	10.2 ±1.0	–	5.8 ±0.3	42.6 ±1.1	–	–
C98883-068	71	–	–	5.6 ±0.5	11.3 ±1.1	12.5 ±2.6	15.0 ±1.0	31.4 ±1.1	–	16.3 ±0.5	7.9 ±0.8	–	–
C97855-042	84	–	–	1.5 ±0.4	7.1 ±1.0	–	16.4 ±1.1	3.2 ±0.6	36.5 ±1.1	3.8 ±0.2	31.5 ±1.0	–	–
C99951-183	271	–	–	9.9 ±0.5	7.8 ±0.8	14.3 ±1.9	11.6 ±0.8	–	–	8.6 ±0.3	47.8 ±1.0	–	–
AD9772-546	378	1.2 ±0.3	–	7.4 ±0.5	10.7 ±1.1	30.3 ±2.9	12.4 ±0.9	13.9 ±1.2	–	8.9 ±0.4	15.2 ±0.9	–	–
C98926-092	1,510	0.7 ±0.3	–	4.4 ±0.4	4.7 ±0.8	20.2 ±2.2	–	25.3 ±1.0	–	8.6 ±0.3	36.1 ±0.9	–	–

[1] Distance to ore was determined by measuring the radial distance between the sample position and the nearest known orebody or resource block.

[2] Minerals belonging to the dolomite-ankerite solid solution series are collectively referred to as ankerite.

[3] Micaceous phases are collectively referred to as illite. Most samples contain two distinct polytypes that could not be quantified separately.

[4] Minerals belonging to the magnesite-siderite solid solution series are collectively referred to as siderite.

amounts of carbonate mineral phases and distance from the clastic ore lenses. However, carbonate concentrations are apparently correlated to distance from the rhyolite footwall. About 45% of the analyzed contact mudstone samples contain members of the dolomite {$CaMg(CO_3)_2$}–ankerite {$CaFe(CO_3)_2$} and (lesser) magnesite {$MgCO_3$}–siderite {$FeCO_3$} solid solutions, compared to only 26% of the more peripheral hangingwall mudstone.

The spatial distribution of ankerite as a major carbonate phase in the carbonaceous mudstone hostrocks suggests that this hydrothermal precipitate formed during or after deposition of the clastic sulphide and sulphosalt mineralization at Eskay Creek. Pervasive carbonate alteration and ankerite veining are abundant in the contact mudstone, but also occur in the hangingwall tens of metres above the stratigraphic interval hosting the bulk of the clastic sulphides (Figure 4). Because stratiform mineralization took place at or very close to the contact between the footwall rhyolite and the overlying mudstone, ankerite in this part of the mine succession records a stage of hangingwall alteration. The ankerite is commonly associated with calcite, but more than one calcite generation has been observed in thin section and significant amounts of calcite may be of regional metamorphic origin. Calcite, unlike ankerite, is increasingly abundant in the peripheral hangingwall samples. Detailed investigation of calcite lattice parameters reveals additional compositional zonation. Calcite with a magnesite component occurs in the proximal contact mudstone, whereas end-member calcite is more common in hangingwall samples. Research carried out so far indicates that zonation of carbonate alteration at Eskay Creek may be the most reliable vector of proximity to hydrothermal upflow zones within tens to hundreds of metres of mineralized zones.

Kaolinite was recognized in the whole-rock XRD patterns of a few samples, all of which also contain abundant ankerite. Thermal stability constraints and observations in natural geothermal systems suggest that kaolinite represents a stable alteration product only at temperatures below 200–300 C (Velde and Kornprobst, 1969), bracketing the temperature of carbonate alteration (and lower greenschist metamorphism). The presence of both phases likely reflects circulation of highly reactive, low-pH, high-CO_2 hydrothermal fluids interacting with hostrocks and diluted by cold seawater (Giggenbach, 1984). Initial geochemical modelling results suggest that fluid alkalinity, mixing with seawater, hostrock chemistry and a temperature decrease associated with fluid migration all contributed to the final alteration assemblage.

The principal sheet silicates detected in the mudstone samples are illite and chlorite. The XRD patterns suggest the presence of two white-mica polytypes, although parameter correlation precluded reliable determination of their relative abundances by the Rietveld method. Total illite concentrations range from <5 to 50 wt. %, whereas chlorite contents range from <5 to 40 wt. %. A number of contact mudstone units have higher illite contents than the hangingwall mudstone, suggesting that illite may, at least in part, be a hydrothermal alteration product. In contrast, chlorite is less abundant in the contact mudstone than in hangingwall samples. Hangingwall samples with abundant chlorite often also contain prehnite and pyrrhotite. The spatial association of prehnite porphyroblasts and basalt intrusions in the hangingwall (Monecke et al., 2005) may suggest that the composition of the mudstone samples is influenced by contact metamorphism.

Pyrite appears equally ubiquitous in the contact and hangingwall mudstone samples investigated. The amount of pyrite varies between <1 and 20 wt. % (Figure 3). Textural evidence suggests that most pyrite is of diagenetic origin. However, the XRD investigations have shown that pyrite with distinctly larger lattice parameters is abundant in proximity to ore, with the enlargement of the unit cell being caused by the presence of As in the crystal structure. These preliminary findings suggest that the As concentration of pyrite could also be used for target vectoring. Minor amounts of sphalerite were detected in many contact and hangingwall mudstone samples, whereas trace amounts of galena and chalcopyrite were only observed proximal to known orebodies.

Principal-Component Analysis

In addition to the minerals identified by whole-rock XRD analysis, the major- and trace-element composition of the mudstone samples was determined by a combination of analytical methods, including X-ray fluorescence and inductively coupled plasma–mass spectrometry (analysis of 22 samples was still incomplete when this paper was written). All mineral and component data were evaluated using principal-component analysis (PCA), which identified 20 statistically significant factors. A varimax rotation was applied to the dataset to give a maximum contrast in loadings, which maximizes variance. Table 2 lists factors by eigenvalue and by the percentage of dataset variance that each factor explains, whereas the cumulative variance is given in the last column. Table 3 lists statistically significant factor loadings and variables for each factor. Factor loadings can be thought of as correlation coefficients whose numerical values reflect the likelihood that variable relationships cannot be explained by random chance. Given a dataset of 158 measurements, each variable carries a single standard deviation of 0.08 (1/[n–1]; n = number of measurements). A normally distributed variable with a factor loading representing one standard deviation has a 32% probability of being explained by random chance, one with two standard deviations has a 4.6% probability, etc. For all

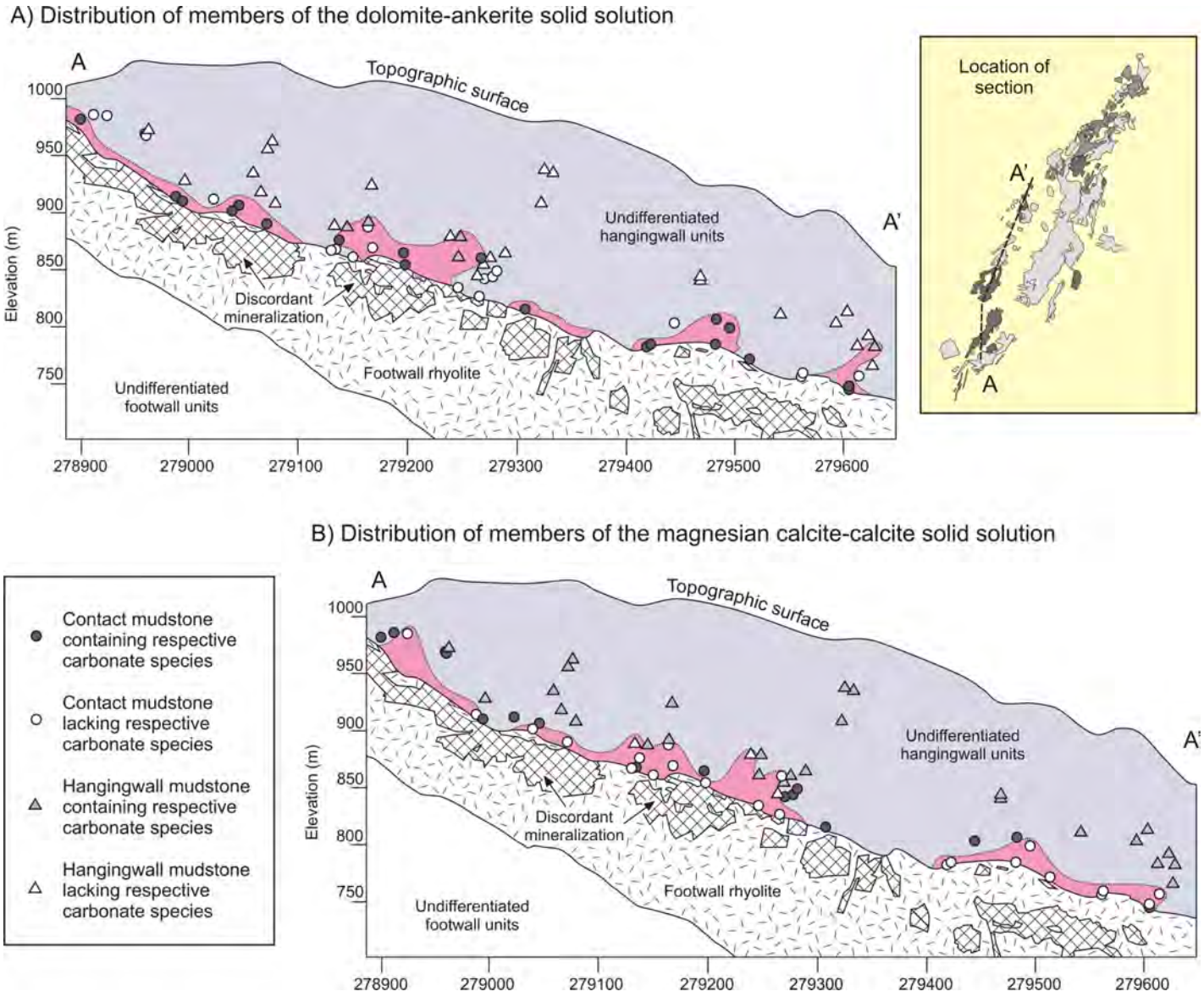

Figure 4. Simplified geological section through the 21C zone, depicting the distribution of carbonate species in the contact and hangingwall mudstones: **A)** dolomite-ankerite solid solutions show a strong spatial association with zones of discordant mineralization in the footwall rhyolite (dotted outline); **B)** calcite is more common in the upper part of the contact mudstone and in the stratigraphically higher hangingwall mudstone. Stratiform mineralization hosted by the mudstone is omitted for clarity. Inset gives the location of the section. Sample positions and locations of zones of discordant mineralization were projected on the section using an envelope of ±100 m.

Table 2. Eigenvalues, percentage of variance and cumulative variance for the first 30 factors identified by principal-component analysis. Based on decreasing variance, geological relevance and number of variables within each factor loading, only the first 20 factors were deemed to be statistically significant.

Factor	Eigen-value	Individual percentage	Cumulative percentage
F1	17.58398	19.76	19.76
F2	7.653404	8.60	28.36
F3	6.185688	6.95	35.31
F4	2.978795	3.35	38.65
F5	6.030588	6.78	45.43
F6	4.544631	5.11	50.54
F7	4.663422	5.24	55.78
F8	3.708948	4.17	59.94
F9	2.922589	3.28	63.23
F10	2.760368	3.10	66.33
F11	2.960360	3.33	69.65
F12	3.716366	4.18	73.83
F13	1.603891	1.80	75.63
F14	1.562975	1.76	77.39
F15	1.783613	2.00	79.39
F16	1.201634	1.35	80.74
F17	1.461582	1.64	82.39
F18	1.314624	1.48	83.86
F19	1.812485	2.04	85.90
F20	1.258079	1.41	87.31
F21	0.883272	0.99	88.30
F22	0.821600	0.92	89.23
F23	0.752652	0.85	90.07
F24	0.726609	0.82	90.89
F25	0.691595	0.78	91.67
F26	0.668764	0.75	92.42
F27	0.607333	0.68	93.10
F28	0.566407	0.64	93.74
F29	0.469700	0.53	94.27
F30	0.413308	0.46	94.73

loadings, only those with three standard deviations (0.24) or greater were chosen as being statistically meaningful.

The PCA techniques proved useful in identifying a number of geologically significant factor loadings that support existing field and laboratory observations, as well as pointing out previously unrecognized patterns. Factor 2, the 'hydrothermal sulphide group', shows a very strong correlation among Cu, Ag, chalcopyrite, galena, Pb, Zn, sphalerite, Sb, Cd and Te, reflecting hydrothermal alteration and mineralization of the mudstone. This element suite is not unlike those of epithermal deposits and is in agreement with the unusual element association observed within the ore zones. Data for Au, As and Hg are not yet available, but all are expected to correlate with this group. In contrast to galena, chalcopyrite and sphalerite, pyrite does not correlate with any of these variables. This mineral is correlated with total S, total Fe and Mo in factor 8, the 'diagenetic sulphide group', supporting a diagenetic origin for much of the pyrite, as observed in the field and in thin section. A weaker inverse correlation with quartz and silica reflects either a variable mudstone protolith siliciclastic and organic fraction or 'dilution' of organic material, pyrite, illite and the feldspathic component of the mudstone with hydrothermal quartz.

Factor 7 suggests a strong relationship between MgO, chlorite and F. A scatter diagram of F/chlorite and MgO/chlorite ratios (Figure 5) demonstrates a strong relationship between F and Mg concentrations in chlorite and, more importantly, shows that the highest concentrations of these elements occur in contact mudstone close to fluid-upflow zones. Additional correlation with Ga, Cd, Zn and Pb provides evidence that compositional trends in chlorite are hydrothermal in nature. Factor 17 confirms the findings of the XRD study that ankerite and kaolinite are correlated with each other, while being inversely correlated with calcite.

Two other factors yield insights that warrant further investigation. Factor 6 points to strong Cs and Rb substitution into the interlayer position of illite. However, for contact mudstone samples with very high illite contents, the substitution ratio appears to vary. Further studies will establish whether Cs and Rb substitution depends on the illite polytype observed by XRD. Factor 9 shows a correlation among organic carbon, Ni and V (and a lesser U, Mo correlation), which points to Ni/V substitution for Mg in chlorophyll porphyrin molecules derived from decaying phytoplankton in the hemipelagic water column (Treibs, 1936). While adding further support for a marine depositional environment, a scatter diagram of Ni/C_{org} versus V/C_{org} ratios (Figure 6) shows both Ni enrichment in carbon-rich hangingwall samples and V enrichment in a number of contact mudstone samples. The trends in both factors 6 and 9 will be further investigated by detailed mineral-composition analysis.

Other geologically significant factor loadings include Th, Ta, Nb, Hf, Zr and Be enrichment in accessory phases such as zircon; rare earth element (except Eu) enrichment in sulphide-bearing samples; Sr and Mn substitution in calcite; and Eu enrichment in fluorapatite.

The preliminary results of this study show that PCA is a useful tool for evaluating multicomponent datasets, and proves to be especially powerful when applied to mineralogical and geochemical data obtained on fine-grained carbonaceous rocks that cannot be readily studied by conventional optical microscopy. Some of the factors identified by PCA add critical statistical support for intuitive conclusions drawn from field and laboratory observations, whereas others point out compositional trends and genetic relationships that would more than likely be missed by

Table 3. Factor loadings and variables for the first 20 factors identified by principal-component analysis. Highly correlated variables are sorted by values, which represent correlation coefficients that reflect strength of relationship. A value of 0.08 represents one standard deviation from random variability. Therefore, a value of at least 0.24 (three standard deviations) deems the correlation 99.7% likely to be statistically meaningful, and not due to natural data variability.

Factor	Correlation	Factor loadings
F1	Strong	Tb (-1.00), Dy (-0.99), Er (-0.99), Gd (-0.99), Ho (-0.99), Sm (-0.99), Tm (-0.99), Y (-0.99), Yb (-0.98), Ce (-0.97), Lu (-0.97), Nd (-0.97), Pr (-0.97), La (-0.96), Tl (-0.94)
	Medium	Sb (-0.53), Eu (-0.44), S (-0.42)
	Weak	U (-0.38), Be (-0.37), $Fe_2O_3^T$ (-0.33)
F2	Strong	Cu (-0.98), Ag (-0.97), chalcopyrite (-0.95), galena (-0.95), Pb (-0.87), Zn (-0.86)
	Medium	Sphalerite (-0.75), Sb (-0.73), Cd (-0.67), Te (-0.62)
	Weak	Ga (-0.40)
F3	Strong	Th (-0.94), Ta (-0.93), Nb (-0.92), Hf (-0.82)
	Medium	Zr (-0.72), Be (-0.60), U (-0.53), Ga (-0.49), Sn (-0.44), Rb (-0.41)
	Weak	Bi (-0.40), illite (-0.38), Al_2O_3 (-0.36), K_2O (-0.30)
F4	Strong	Rutile (-0.83), Cr (-0.82)
	Medium	Co (-0.61), TiO_2 (-0.55), Sc (-0.49)
	Weak	$Fe_2O_3^T$ (-0.35), chlorite (-0.32)
F5	Medium	SiO_2 (-0.75), quartz (-0.44)
	Medium	Barite (0.45), ankerite (0.58), Sr (0.69), MnO (0.79)
	Strong	LOI (0.85), calcite (0.87), CaO (0.90), CO_2 (0.95)
F6	Strong	Cs (-0.88), Illite (-0.83)
	Medium	Anatase (-0.66), Rb (-0.58), Al_2O_3 (-0.48)
	Weak	Gypsum (-0.38), K_2O (-0.38), TiO_2 (-0.37), Zr (-0.36), Sc (-0.33), F (-0.32)
	Weak	Chlorite (0.32)
F7	Weak	SiO_2 (-0.34)
	Weak	Pb (0.34), dolomite (0.38)
	Medium	Zn (0.44), Cd (0.51), Ga (0.52), sphalerite (0.56), F (0.70), chlorite (0.74)
	Strong	MgO (0.84), anglesite (0.86)
F8	Strong	Pyrite (-0.89), S (-0.83)
	Medium	$Fe_2O_3^T$ (-0.76), Mo (-0.44)
	Weak	Quartz (0.35), SiO_2 (0.37)
F9	Strong	Ni (-0.82), C (-0.80)
	Medium	V (-0.77), U (-0.42)
	Weak	Mo (-0.31)
F10	Medium	Eu (0.69)
	Strong	Apatite (0.95), P_2O_5 (0.96)
F11	Strong	Plagioclase (-0.95), Na_2O (-0.94)
	Medium	Anatase (-0.37), Sr (-0.36)
	Medium	Quartz (0.36)
F12	Strong	Microcline (-0.90)
	Medium	K_2O (-0.77), Al_2O_3 (-0.57), Sc (-0.56), TiO_2 (-0.53), Ba (-0.43)
	Weak	Rb (-0.38), Zr (-0.34), Hf (-0.32), Co (-0.31)
	Medium	Quartz (0.55)
F13	Medium	In (-0.79), Bi (-0.78)
	Weak	Siderite (-0.30)
F14	Medium	Dolomite (-0.63), siderite (-0.60)
	Weak	Be (-0.31)
	Weak	Gypsum (0.38)
F15	Strong	Prehnite (-0.87)
	Medium	Pyrrhotite (-0.70)
F16	Strong	Magnesite (-0.90)
	Medium	Kaolinite (-0.50)
F17	Medium	Barite (-0.59)
	Weak	Ba (-0.31), calcite (-0.31)
	Medium	Kaolinite (0.52), ankerite (0.63)
F18	Medium	Ba (0.59)
	Strong	Armenite (0.82)
F19	Weak	Pb (0.30)
	Medium	Te (0.59)
	Strong	Jarosite (0.85)
F20	Medium	Bassanite (-0.72), gypsum (-0.42)
	Weak	Mo (-0.40)

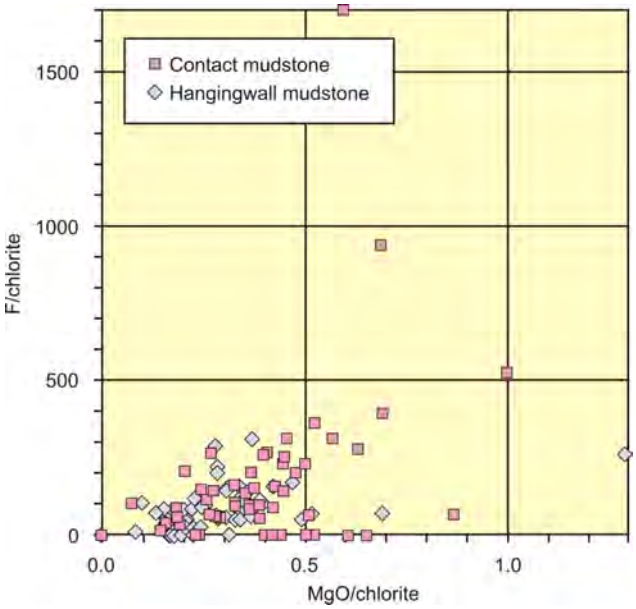

Figure 5. Scatter diagram of F/chlorite versus MgO/chlorite ratios, showing strong correlation between F and Mg concentrations in chlorite. Highest F and Mg concentrations occur in samples collected proximal to mineralization.

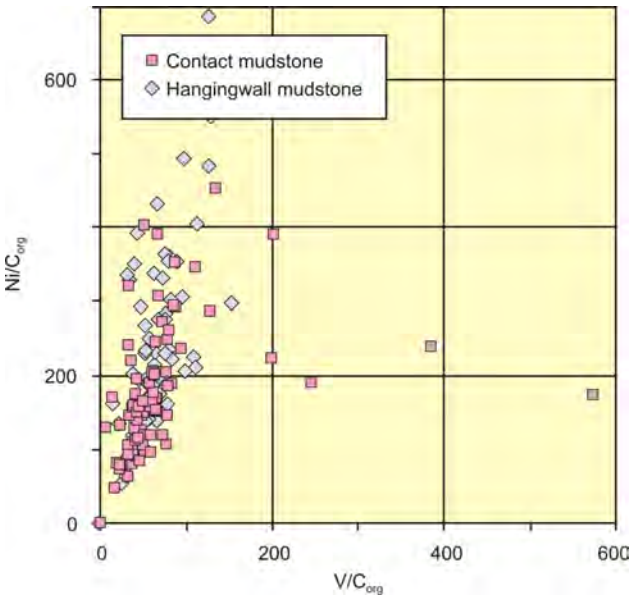

Figure 6. Scatter diagram of Ni/C_{org} ratio versus V/C_{org} ratio. High correlation reflects substitution of these metals for Mg in the porphyrin ring-structure of chlorophyll molecules derived from decaying phytoplankton. Some hangingwall samples show Ni enrichment, whereas a group of contact mudstone units shows a relative enrichment in V.

traditional univariate and bivariate analysis of such a large dataset.

Potential Vectors to Ore

A number of observed compositional trends in the mudstone represent potential vectors to ore, and will the subject of further studies. The following minerals and component concentrations all increase with increasing alteration intensity proximal to mineralization:

- ankerite and kaolinite (end-member calcite increases in distal rocks)
- Mg and Fe concentrations in all carbonates
- As concentrations in pyrite
- Mg and F ratios in chlorite
- Cs (and possibly Rb) substitution ratios in illite
- V/C_{org} ratios

Future work will include microanalytical studies on the carbonate minerals and on pyrite, chlorite and illite. Additional multivariate investigations will involve addition of geochemical parameters (i.e., Au, As, Se and Hg), detailed plotting of factor scores to understand spatial controls on data variance, principal-component regression (PCR) with spatial variables, and protolith cluster analysis.

Acknowledgments

The authors gratefully acknowledge Geoscience BC, Barrick Gold Corporation, the Michael-Juergen-Leisler-Kiep Foundation and the German Research Foundation for supporting this study. This study would not have been possible without the help provided by T. Roth, M.D. Hannington and R.M. Tosdal. R. Kleeberg is thanked for analytical support. We are grateful to M. Hitzman for reviewing this paper and for his insightful comments that helped improve an earlier version of the manuscript.

References

Alldrick, D.J., Nelson, J.L., Barresi, T., Stewart, M.L. and Simpson, K. (2005): Geology of the Upper Iskut River area, British Columbia; BC Ministry of Forests, Mines and Lands, Open File 2006-2, scale 1:100 000.

Barrett, T.J. and Sherlock, R.L. (1996): Geology, lithogeochemistry and volcanic setting of the Eskay Creek Au-Ag-Cu-Zn deposit, northwestern British Columbia; Exploration and Mining Geology, v. 5, p. 339–368.

BC Geological Survey (2010): MINFILE BC mineral deposits database; BC Ministry of Forest, Mines and Lands, URL <http://minfile.ca/> [November 2010].

Britton, J.M., Blackwell, J.D. and Schroeter, T.G. (1990): #21 zone deposit, Eskay Creek, northwestern British Columbia; BC Ministry of Forests, Mines and Lands, Exploration in British Columbia 1989, p. 197–223.

Childe, F. (1996): U-Pb geochronology and Nd and Pb isotope characteristics of the Au-Ag rich Eskay Creek volcanogenic massive sulfide deposit, British Columbia; Economic Geology, v. 91, p. 1209–1224.

Gabrielse, H., Monger, J.W.H., Wheeler, J.O. and Yorath, C.J. (1991): Morphogeological belts, tectonic assemblages and terranes; *in* Geology of the Cordilleran Orogen in Canada, H. Gabrielse and C.J. Yorath (ed.), Geological Survey of Canada, Geology of Canada, no. 4, p. 15–28 (also Geological Society of America, Geology of North America, v. G-2).

Giggenbach, W.F. (1984): Mass transfer in hydrothermal alteration systems—a conceptual approach; Geochimica et Cosmochimica Acta, v. 48, p. 2693–2711.

Hannington, M.D., Poulsen, K.H., Thompson, J.F.H. and Sillitoe, R.H. (1999): Volcanogenic gold in the massive sulfide environment; Reviews in Economic Geology, v. 8, p. 325–356.

Kley, R.J. (1968): Distribution of selected trace elements in rocks; U.S. Army Corps of Engineers, Nuclear Cratering Group, p. 1–68.

Monecke, T., Gale, D., Roth, T. and Hannington, M.D. (2005): The submarine volcanic succession hosting the massive sulfide and sulfosalt Eskay Creek deposit, Canada; *in* Mineral Deposit Research: Meeting the Global Challenge, Y. Mao and F.P. Bierlein (ed.), Proceedings of the 8th Biennial SGA (Society for Geology Applied to Mineral Deposits) Meeting, August 18–21, 2005, Beijing, Peoples Republic of China, Springer, p. 655–658.

Roth, T., Thompson, J.F.H. and Barrett, T.J. (1999): The precious metal-rich Eskay Creek deposit, northwestern British Columbia; Reviews in Economic Geology, v. 8, p. 357–373.

Treibs, A.E. (1936): Chlorophyll- und Huminderivate in organischen Mineralstoffen; Angewandte Chemie 1936, v. 49, p. 682–686.

Velde, B. and Kornprobst, J. (1969): Stabilité des silicates d'alumine hydratés; Contributions to Mineralogy and Petrology, v. 21, p. 63–74.